Non-optical Water Quality Retrieval from Zhuhai-1 OHS Hyperspectral Images in Taipu River

Yukun Lin[a,b], Yaojen Tu[a,b,*], Wenpeng Lin[a,b,*], Weiyue Li [a,b], Qianwen Cheng [a,b]

a School of Environmental and Geographical Sciences, Shanghai Normal University, Shanghai 200234, China

b Yangtze River Delta Urban Wetland Ecosystem National Field Scientific Observation and Research Station, Shanghai 200234, China

Abstract

Hyperspectral remote sensing is thought to be a useful technology for assessing the condition of inland waters. However, non-optically active water quality parameters are rarely explored in hyperspectral remote sensing applications, despite they are highly valued in the aquatic environment condition. This study intends to evaluate the performance of non-optically active water quality parameters using Zhuhai-1 OHS hyperspectral imagery. Focusing on total nitrogen (TN), total phosphorus (TP), ammonia nitrogen (NH_3-N) and nitrate-nitrogen (NO_3-N) in Taipu River, we constructed empirical models to evaluate the precision of water quality inversion from OHS by comparing with Sentinel-2, and determined the sensitive bands of different water quality parameters. The final results showed that the polynomial model based on OHS had the greatest potential in retrieving TN, TP and NH_3-N concentration, and the R^2 was 0.9678, 0.7924, 0.7682 respectively. The combination of R(510)/R(820) and R(700)/R(806), R(940)/R(820) and R(806)/R(926), R(709)/R(806) and R(746)/R(620) were most sensitive to TN, TP and NH_3-N respectively. The OHS and Sentinel-2 both had potential in retrieving NO_3-N. The R^2 was 0.9791 from OHS and was 0.9513 from Sentinel-2. The sensitive bands of NO_3-N were R(596)/R(665) and R(466)/R(580) from OHS, and Red Eage3/Blue and SWIR1/Blue from Sentinel-2. We also analyzed the drivers of the spatial distribution of water quality in the Taipu River based on redundancy analysis (RDA), the results showed negative impacts of farmland and urban land on water quality, and beneficial impacts of forest land on water quality. This study represented a promising first step in hyperspectral remote sensing for retrieving inland non-optically active water quality parameters utilizing Zhuhai-1.

Keywords: Zhuhai-1 satellite, non-optical parameters, water quality, Taipu River, empirical model

I. INTRODUCTION

The Taipu River serves as a major drinking water supply route for the Yangtze River Delta Ecology and Greenery Integration Development Demonstration Zone in China. The upstream is linked to the East Taihu Lake Water Source, while the downstream is linked to Shanghai Jinze Reservoir and the Jiashan Changbaidang Drinking Water Source Protection Area(H. Zhu, 2018). It serves as a key canal for flood discharge and shipping, moreover, serves as a source of drinkable water, which needs to meet strict criteria for water quality and ecological balance. Along the Taipu River, the dense populations and considerable industries such as chemical, textile, printing and dyeing, polyester, will deteriorate water quality(Y. Wang et al., 2021). Recently, pollution occurrences in the Taipu River have sparked considerable concern. Therefore, analyzing the spatiotemporal distribution features of the Taipu River's water quality is increasingly critical.

Four significant non-optical parameters, TN, TP, NH_3-N, and NO_3-N, have been extensively investigated to represent the eutrophication of rivers and lakes, which will cause a critical water pollution issue in many countries like degrading functioning and endangering water security (X. Chen et al., 2018; Liang et al., 2018; Lv & Wu, 2021; Mararakanye et al., 2022). Traditionally, in-situ measurements and the collection of water samples are the major approaches for monitoring water quality. Even if these measurements are accurate for a specific area, they cannot provide a regional perspective on water quality (Ross et al., 2019; D. Sun et al., 2014). In order to represent the spatial distribution and seasonal changes in water quality components, remote sensing technology has been adopted due to the benefits of spatial and temporal coverage (Kallio et al., 2001; K. Shi et al., 2018; Xu et al., 2016). Different sensors with visible and infrared wavelengths may be utilized to monitor water quality due to high-frequency data collecting and large-scale coverage.

Generally, the spectral resolution of data sources for water quality retrieval can be classified into two categories: multispectral data and hyperspectral data (H. Yang et al., 2022). In the field of multispectral water quality retrieval, many scholars monitor the TN and TP using National Oceanic and Atmospheric Administration (NOAA) Advanced Very High Resolution Radiometer (AVHRR) imagery (Y. Wang et al., 2016), Landsat series data (H. Guo et al., 2022), MODIS data (Arıman, 2021), IKONOS imagery (J. Liu et al., 2015) and Sentinel-2 imagery (H. W. Guo et al., 2021). The accuracy (R^2) range of TN/TP in references is from 0.36 to 0.87 and 0.59 to 0.96 individually. The scenes of high-resolution multispectral SPOT-5 (Satellite Pour l'Observation de la Terre) data (X. L. Wang et al., 2011), Landsat-8 OLI satellite data (C. Liu et al., 2019), Sentinel-2 imagery (Dong et al., 2020) and Unmanned Aerial Vehicle (UAV) multispectral data(B. T. Chen et al., 2021) were used to establish the relationship between the surface reflectance and NH_3-N. The accuracy (R^2) range of NH_3-N in references is from 0.69 to 0.88. The multispectral technology has no relevant results in the monitoring of NO_3-N in inland rivers. Generally, due to spectral resolution limitations, the overall precision of multispectral remote sensing water quality is relatively low.

In the field of hyperspectral water quality retrieval, hyperspectral remote sensing data from the ground-based and proximal hyperspectral imager (Q. Cao et al., 2022; X. Sun et al., 2022), the handheld Analytical Spectral Devices (ASD) field spectrometer (S. Wang et al., 2022) and the UAV equipped with a hyperspectral imaging sensor (Song et al., 2014), were applied to water quality retrieval of TN and TP. The accuracy (R^2) is higher than multispectral with the range of TN/TP in references from 0.59 to 0.90 and 0.73 to 0.93 individually. The ground-based hyperspectral data(Q. Cao et al., 2022) and UAV-borne hyperspectral imagery (Wang et al., 2021) were used to estimate water quality retrieval of NH_3-N. The accuracy (R^2) is higher than multispectral with the range from 0.83 to 0.95. The ground-based hyperspectral data was used to estimate water quality retrieval of NO_3-N. The accuracy (R^2) range of NO_3-N in reference is 0.77. However, focusing just on the spectrum makes it challenging to understand the spatial distribution of water quality along the whole river channel (Wang et al., 2021). In addition, non-satellite remote sensing data sources that rely on aircraft measurements are more expensive and requires superb UAV operation skills. Moreover, hyperspectral satellites can also solve the problems of synonyms spectrum in multispectral data due to its numerous bands (Y. Cao et al., 2018). These days, the Orbita Hyperspectral Satellites (OHS) with fine spectral, spatial, and temporal resolution

are available. However, the applicability of monitoring inland water quality parameters utilizing OHS data has not been well investigated, particularly for the non-optically active water quality parameters.

The study aims to retrieve TN, TP, NH_3-N and NO_3-N concentrations in the Taipu River from OHS data, as well as to investigate the performance of the empirical model based on the single band and band ratio. In the study, the case study area and relevant data sets were introduced initially. Then, the waterbody was extracted and the cloud and dark surface in the images were detected and removed. Next, we presented four empirical band arithmetic algorithms (linear, logarithmic, exponential and polynomial) for TN, TP, NH_3-N and NO_3-N retrieval. The performances on the Sentinel-2A multispectral image and OHS hyperspectral images were compared and the sensitive features were investigated respectively. The optimal model with the best-performed image were used to create maps of water quality concentration in the Taipu River. The results will be explained and discussed then. Finally, we draw some conclusions.

II MATERIALS

A. Study Sites and in Situ Data

The Taipu River is a part of the Taihu Lake Basin's river network. Additionally, it is also strongly connected to the surrounding water network, which comprises 205 small to medium-sized lakes, and is impacted by the influx of tributaries on both sides of the river. The length and width of the Taipu River are 57.2 kilometers and 200 meters, respectively. The flow rate is 0.6 m/s on average, and the flow is about 300 m^3/s (Yao et al., 2015). Along this canal are tens of thousands of textile factories as well as 95 centralized sewage disposal facilities. (Yao et al., 2014). Therefore, Taipu River is a typical area for water quality research.

As shown in Figure 1, a total of 12 in-situ samples of water quality parameters were collected in Taipu River. The field measurements include total nitrogen (TN), total phosphorus (TP), ammonia nitrogen (NH_3-N) and nitrate-nitrogen (NO_3-N). The samples are all concentrated at the intersection of the major streams and regional functional zones. The sampling points were measured on July 7, 2021, since the synchronized OHS and Sentinel-2 images corresponded to the Taipu River field experiments were acquired in July 6, 2021 and July 7, 2021 respectively.

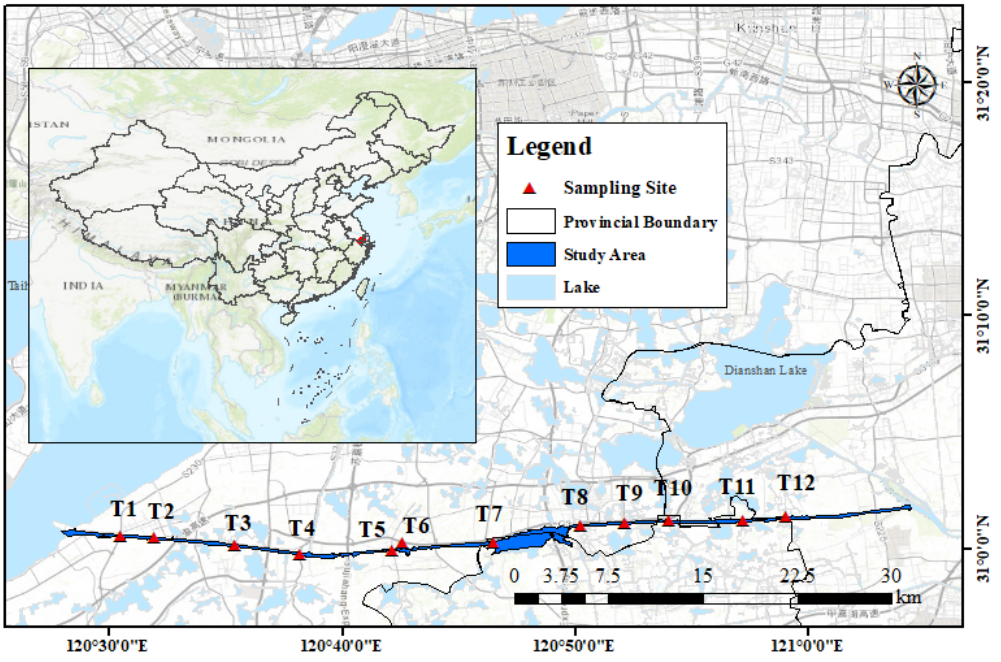

Figure 1 Map of sampling sites for water quality inversion of Taipu River

B. Remote Sensing Data

The Zhuhai-1 mission, developed by Zhuhai Orbita Control Engineering Ltd. (https://www.myorbita.net/), was China's first commercial microsatellite constellation. The Zhuhai-1 mission includes 34 microsatellites: 12 video satellites (OVS-1/2/3/4), two high spatial resolution satellites (OUS), two radar satellites (SAR), eight infrared satellites (OIS), and ten hyperspectral satellites (OHS)(Qin et al., 2022). The Orbita Hyperspectral Satellites (OHS) comprise 32 bands with a wavelength range of 400 to 1000 nm, a spatial resolution of 10 m, and a spectral resolution of 2.5 nm. To date, the single OHS has a temporal resolution of 6 days, and the combined temporal resolution of 8 OHSs is reduced to about 1 day(Zhong et al., 2021). The OHS has significant promise for monitoring inland water quality due to its high spatial, spectral, and temporal resolutions. The preprocessing of OHS includes band combination, radiometric calibration, atmospheric correction, and orthorectification, which converts the raw images into surface reflectance with precise geometric positioning, laying the groundwork for the subsequent inversion of water quality parameters. All the preprocessing steps are completed in ENVI 5.3.

Sentinel-2 Level-1C (L1C) MSI data could be downloaded from Sentinels Scientific Data Hub (https://scihub.copernicus.eu/). Sentinel-2 comprises 13 spectral bands with a wavelength range of 430 to 2190 nm. The 5 days revisit time of the twin Sentinel-2 satellites is crucial because of the water quality changes caused by weather condition. The spatial resolution of Sentinel-2 is 10m, 20m and 60m, which means even small river and lakes can be studied(Toming et al., 2016). The Sen2Cor plug-in in the SNAP (SeNtinel Application Platform) toolbox was used for atmospheric correction to obtain the reflectance level images. The images then resampled to 20m resolution utilizing the Sentinel-2 Resampling technique also provided by SNAP Toolbox(J. Shi et al., 2022). Table 1 summarized the key technological characteristics of the OHS and Senitnel-2.

137 Table 1 Center Wavelength and Spatial Resolution of OHS and Sentinel-2

Channel	OHS			Sentinel-2		
	Center wavelength (nm)	Band Number	Spatial resolution (m)	Center wavelength (nm)	Band Number	Spatial resolution (m)
Blue	443	B01	10	490	b2	10
	466	B02				
	490	B03				
Green	500	B04	10	560	b3	10
	510	B05				
	531	B06				
	550	B07				
	560	B08				
Red	580	B09	10	665	b4	10
	596	B10				
	620	B11				
	640	B12				
	665	B13				
Red Edge1	670	B14	10	705	b5	20
	686	B15				
	700	B16				
	709	B17				
Red Edge2	730	B18	10	740	b6	20
	746	B19				
Red Edge3	760	B20	10	783	b7	20
	776	B21				
	780	B22				
NIR （Sentinel-2）	806	B23	10	842	b8	10
	820	B24				
	833	B25				
Narrow NIR （Sentinel-2）	850	B26	10	865	b8a	20
	865	B27				
NIR (OHS)	880	B28	10	—	—	—
	896	B29				
	910	B30				
	926	B31				
	940	B32				
SWIR1	—	—	—	1610	b11	20
SWIR2	—	—	—	2190	b12	20

III. METHODS

A. Waterbody Extraction

The water mask of Taipu River was derived from a vector dataset, the Open Street Map (OSM). OSM contains a huge amount of objects related to water and it is widely used in environmental applications including the extraction of rivers, lakes, and shoreline boundaries for hydrological analysis(Donchyts et al., 2016; Marshak et al., 2020). In this study, we merged all the OSM vectors in Taipu River into a single layer and corrected the typographic errors through the visual interpretation process of the OHS image. All the steps are performed in ArcMap 10.7.

B. Cloud Detection and Dark Surface Detection

The spectral bands of optical sensors are substantially impacted by clouds(Irish et al., 2006), in addition, the calculation of spectral indices might suffer from their existence(Huete et al., 2002). Therefore, identifying clouds in optical images is often a prerequisite for their use(Z. Zhu et al., 2015). There was no cloud in the OHS image but sparse cloud in the Sentinel-2 image. Fmask 4.0 was applied to detect cloud for Sentinel-2 image by integrating auxiliary data, new cloud probabilities, and novel spectral-contextual features, which outperformed Sen2Cor 2.5.5 in terms of overall accuracy by 7%(Qiu et al., 2019).

Taipu River, the urban surface water, is easily affected by noise in heterogeneous urban scenes, such as soil, roadways and cloud shadows(X. Yang et al., 2018). The water index, AWEIsh, was calculated to enhance the difference between water and non-water bodies(X. Yang et al., 2018). The AWEIsh tends to have positive values for water bodies, whereas negative values for soil and cloud shadows. The empirical threshold of 0.214 was adopted in this study. The waterbody of Sentinel-2 was conducted by combination of cloud detection result and non-water dark surfaces .The result of cloud/cloud shadow removal is presented in Figure 2.

Figure 2 Water mask for the true color composite image (Red, green and blue bands) of Sentinel-2 scenarios (water mask in blue).

C. Water Quality Inversion

The water quality inversion are following three steps. First, from each sample point in the Taipu River, the mean value of 3×3 cloud-free pixels were calculated for avoiding noise effectively. Then, the single band and band ratio of OHS and Sentinel-2 were selected to create the effective spectral information expression and to provide a framework for the qualitative and quantitative assessment of water quality. Finally, linear regression model was established by linear, logarithmic, exponential and polynomial, which was constructed by Formulas (1)-(4). Model inversion was mainly realized through MATLAB 2021a.

$$Linear \propto a \times R_{rs} + b \quad (1)$$

$$Logarithmic \propto a \times log_{10} R_{rs} + b \quad (2)$$

$$Exponential \propto a \times e^{b \times R_{rs}} \quad (3)$$

$$Polynomial \propto a \times R_{rs}(\lambda) + b \times R_{rs} + c \quad (4)$$

where R_{rs} represents band or band ratio of remote sensing images and a, b and c are the fitting coefficients.

D. Validation and Evaluation

The predictive performance of the linear regression model is primarily determined by the square of the correlation coefficient (R^2) and the Root Mean Squared Error (RMSE), which are calculated between the measured values and predicted values. The best models for assessing water quality are those with the highest R^2 value and the lowest RMSE. The followings are the equations of measurements:

$$RMSE = \sqrt{\sum_{i=1}^{n}(y_i - y_i')^2 / n} \quad (5)$$

$$R^2 = 1 - \sum_{i=1}^{n}(y_i - y_i')^2 / \sum_{i=1}^{n}(y_i - \bar{y}_i)^2 \quad (6)$$

where y_i and y_i' are the observed and predicted value for the *i*th observation; $\bar{y}_i$ is the average observed value; *n* is the number of validation samples.

IV. RESULTS

A. Analysis of Measured Water Quality

The statistics of the measured water quality in this experiment are listed in Table 2, which summarizes the measured water quality parameters in this experiment. The range of TN concentrations was from 0.972 to 2.192 mg/L, and the mean (± standard deviation) was 1.457 ± 0.371 mg/L. According to the "Surface Water Environmental Quality Standard" (GB 3838-2002) in China, the average value of TN met the requirement of water class IV. The range of TP concentrations was from 0.03 to 0.14 mg/L, and the mean (± standard deviation) was 0.075 ±0.034 mg/L. The average value of TP met the requirement of water class III. The range of NH_3-N concentrations was from 0.25 to 1.45 mg/L, and the mean (± standard deviation) was 0.537 ±0.307 mg/L. The average value of NH_3-N met the requirement of water class III. Overall the water quality was below Class IV. Tthe overall water quality of the Taipu River tends to be the same as previous years.

Table 2 Summary of water quality concentrations of Taipu River sampling points.

	TN (mg/L)	TP (mg/L)	NH_3-N (mg/L)	NO_3-N (mg/L)
Maximum	2.192	0.14	1.45	1.257
Minimum	0.972	0.03	0.25	0.001
Mean	1.457	0.075	0.537	0.415
Standard deviation	0.371	0.034	0.307	0.42

B. Model Performance based on OHS and Sentinel-2

As shown in Table 3, the polynomial model had the best accuracy for modeling TN, TP, NH_3-N, and NO_3-N concentrations based on OHS, and their R^2 was 0.9678, 0.7924, 0.7682 and 0.9791, the corresponding RMSE was 0.0520 mg/L, 0.0135 mg/L, 0.051 mg/L and 0.0566 mg/L. The combination of green/NIR and Red edge1/NIR bands exhibited significant relationships with TN. The combination of NIR(940nm)/NIR(820nm) and NIR(806nm)/NIR(926nm) bands exhibited significant relationships with TP. The combination of Red edge1/NIR and Red edge2/Red bands exhibited significant relationships with NH_3-N. The combination of Red(596nm)/Red(665nm) and Blue/Red bands exhibited significant relationships with NO_3-N. From Figure 3, a strong linear relationship was shown between the measured and the predicted concentrations of TN, TP, NH_3-N and NO_3-N, which also indicated that polynomial model had good prediction accuracy and was appropriate for OHS remote sensing inversion.

Table 3 Statistics (R^2 and RMSE) for TN, TP, NH_3-N and NO_3-N concentrations based on OHS image.

	Model	Band ratio	R^2	RMSE (mg/L)
TN	Linear	B03/B05	0.6897	0.1616
	Exp	B02/B09	0.6946	0.1603
	Log	B03/B05	0.6892	0.1617
	Polynomial	B05/B24、B16/B23	**0.9678**	**0.0520**
TP	Linear	B24/B23	0.4028	0.0228
	Exp	B24/B23	0.4159	0.0226
	Log	B24/B23	0.3898	0.0231
	Polynomial	B32/B24、B23/B31	**0.7924**	**0.0135**
NH_3-N	Linear	B23/B21	0.3055	0.0883
	Exp	B25/B27	0.3479	0.0856
	Log	B03/B05	0.2923	0.0891
	Polynomial	B17/B23、B19/B11	**0.7682**	**0.051**
NO_3-N	Linear	B10/B16	0.7458	0.1974
	Exp	B10/B16	0.757	0.193
	Log	B10/B16	0.7356	0.2013
	Polynomial	B10/B13、B02/B09	**0.9791**	**0.0566**

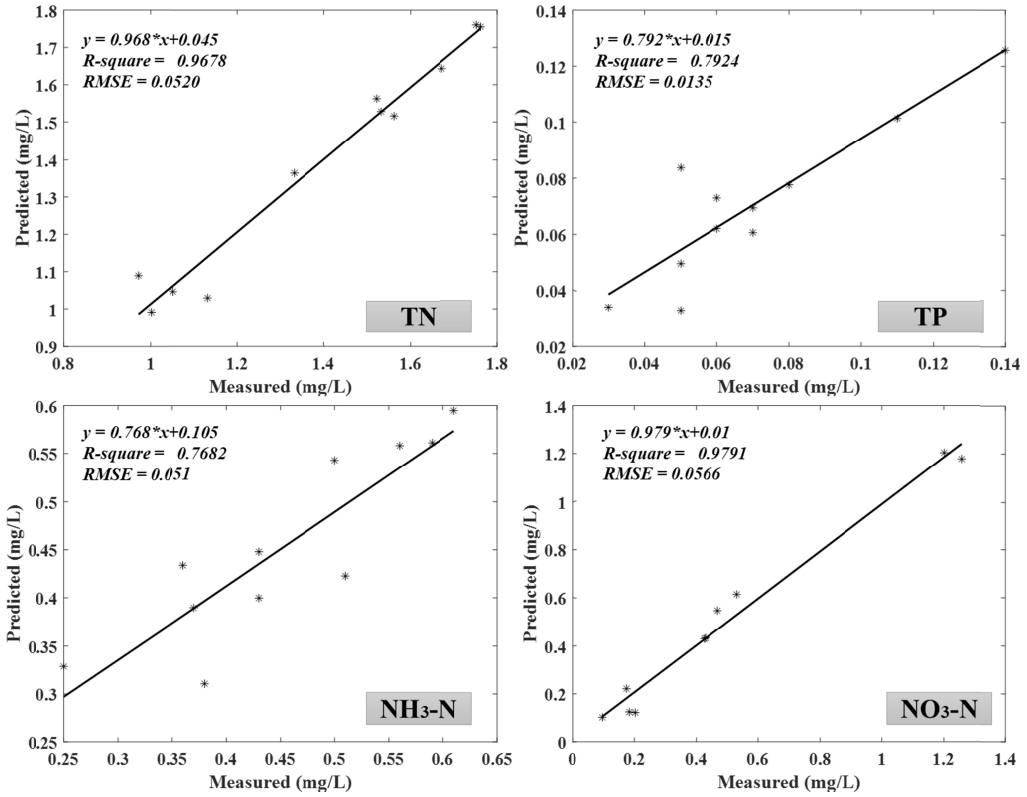

Figure 3 Accuracy of linear relationship between measured and predicted concentrations and RMSE of TN, TP, NH_3-N and NO_3-N from OHS image.

Compared to water quality estimation results using OHS images, a significant decrease performance was shown from Sentinel-2 image. It can be seen from Table 4 that the polynomial model had the best accuracy for modeling TN, TP, NH_3-N, and NO_3-N concentrations based on Sentinel-2, and their R^2 was 0.8854, 0.4192, 0.6601 and 0.9513, the corresponding RMSE was 0.1028 mg/L, 0.0231 mg/L, 0.0622 mg/L and 0.0878 mg/L. The combination of NIR/Narrow NIR and Red edge1/Red bands exhibited significant relationships with TN. The combination of Red edge3/Blue and SWIR1/Blue bands exhibited significant relationships with NO_3-N. From Figure 4, a strong linear relationship was shown between the measured and the predicted concentrations of TN and NO_3-N, which indicated that polynomial model had good prediction accuracy and was appropriate for TN and NO_3-N inversion from Sentinel-2 images. However, we can also observe that there was a large difference between the predicted value and the observed value of TP and NH_3-N, indicating that the prediction errors are relatively large.

Table 4 Statistics (R^2 and RMSE) for TN, TP, NH_3-N and NO_3-N concentrations based on Sentinel-2 image.

	Model	Band ratio	R^2	RMSE (mg/L)
TN	Linear	b7/b8	0.8156	0.1304
	Exp	b7/b8	0.8173	0.1298
	Log	b7/b8	0.8138	0.1310
	Polynomial	b8/b8a、b5/b4	**0.8854**	**0.1028**

TP	Linear	b4/b2	0.1168	0.0284
	Exp	b4/b2	0.1195	0.0284
	Log	b4/b2	0.1133	0.0285
	Polynomial	b6/b8a、b8a/b2	**0.4192**	**0.0231**
NH_3-N	Linear	b4/b3	0.4156	0.0816
	Exp	b4/b3	0.4159	0.0815
	Log	b4/b3	0.4150	0.0816
	Polynomial	b6/b7、b4/b3	**0.6601**	**0.0622**
NO_3-N	Linear	b8a/b11	0.3112	0.3301
	Exp	b2/b12	0.3474	0.3213
	Log	b8a/b11	0.2978	0.3333
	Polynomial	b7/b2、b11/b2	**0.9513**	**0.0878**

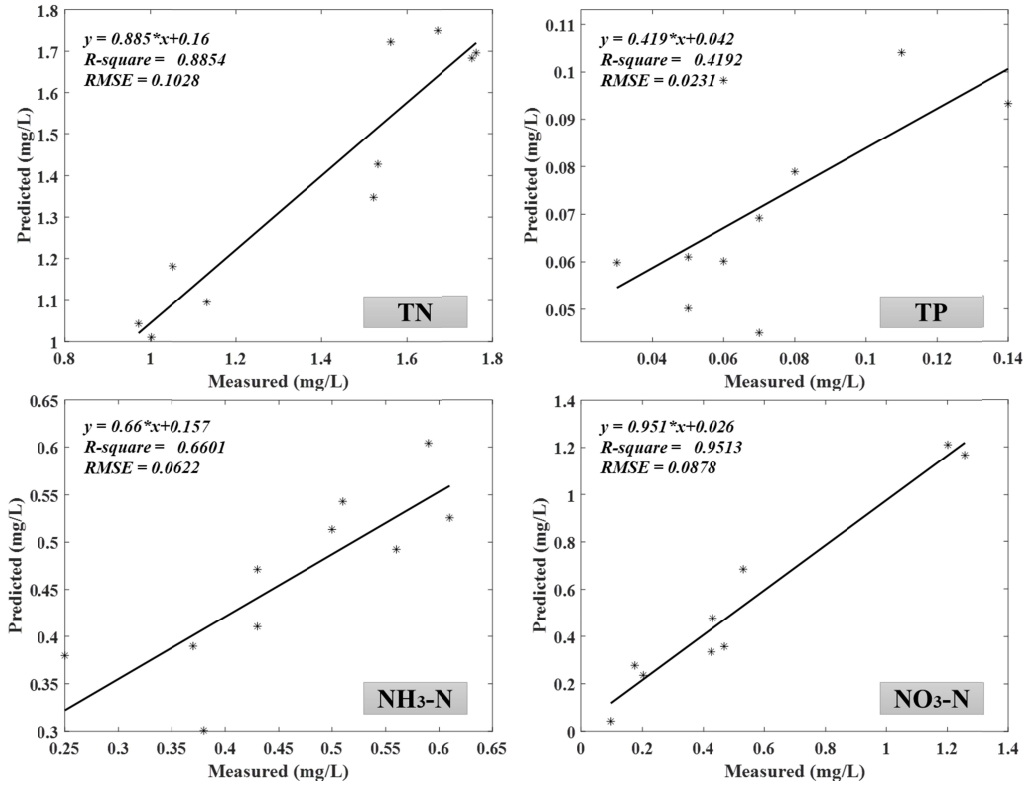

Figure 4 Accuracy of linear relationship between measured and predicted concentrations and RMSE of TN, TP, NH_3-N and NO_3-N from Sentinel-2 image.

C. Optimal Model Application in Best-performed Images

Figure 5 shows the results of TN, TP, NH_3-N and NO_3-N inversion of OHS image in the Taipu River using the best fitting model (polynomial). An obvious weakness of the polynomial model is that the negative and anomaly positive value will exist in the result. Therefore, the

inversion results exclude negative values and values outside the 95th percentile. The inversion results showed that the maximum value of TN in the Taipu River is 1.66 mg/L, and the minimum value is 0.0067 mg/L, which is basically consistent with the in-situ measurements (TN max = 2.192 mg/L, TN min = 0.972 mg/L). The maximum value of TP in the Taipu River is 0.15 mg/L, and the minimum value is 0.001 mg/L, which is basically consistent with the in-situ measurements (TP max = 0.14 mg/L, TP min = 0.03 mg/L). The maximum value of NH_3-N in the Taipu River is 5.2 mg/L, and the minimum value is 0.001 mg/L, which is higher than in-situ measurements (NH_3-N max = 1.45 mg/L, NH_3-N min = 0.25 mg/L). However, the mean value of NH_3-N is 0.7718 mg/L, which indicates the NH_3-N concentration is low in the Taipu River. The maximum value of NO_3-N in the Taipu River is 1.32 mg/L, and the minimum value is 0.001 mg/L, which is basically consistent with the in-situ measurements (NO_3-N max = 1.257 mg/L, NO_3-N min = 0.001 mg/L).

The spatial distribution of TN and NO_3-N shows a general trend of deterioration in the water quality of the Taipu River from upstream to downstream. The TP and NH_3-N concentration in Taipu River is evenly distributed. It also can be seen that the water quality parameter of TN in the upper reaches is class III and in the lower reaches is class IV. Moreover, the water quality parameter of TP is class III, and the water quality classification results for NH_3-N is class IV.

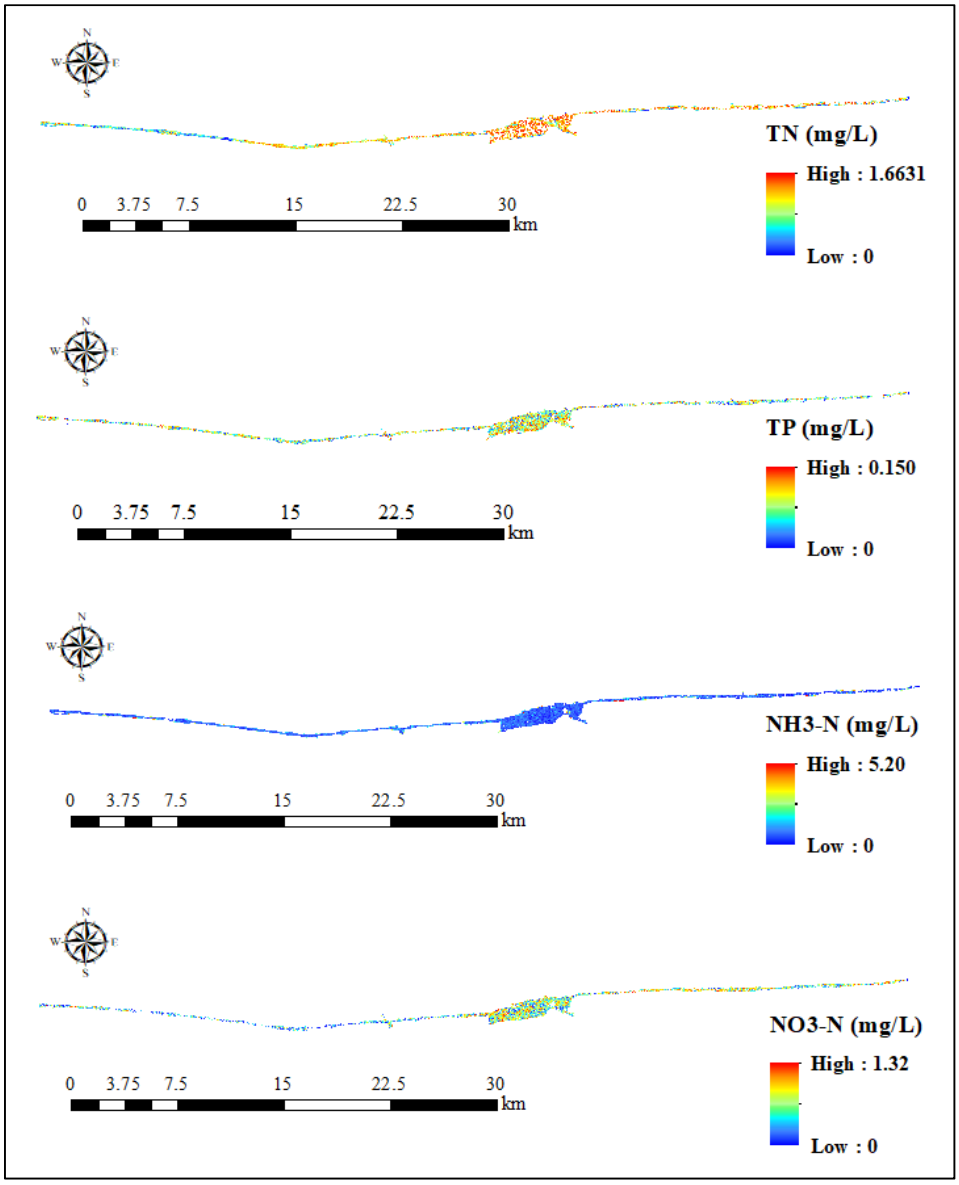

Figure 5 Spatial patterns of TN (a), TP (b), NH_3-N (c) and NO_3-N (d) in Taipu River.

V. DISCUSSION

A. Driving Forces of Water Quality in the Taipu River

As the Figure 6 showed, the upper reaches of the Taipu River is occupied mainly by cropland; the middle reaches of the Taipu River is occupied mainly by impervious surface; the lower reaches of the Taipu River is dominated by forest. In this study, 38 random points was selected evenly distributed along the Taipu River to analyze the drivers of the water quality. The land cover percentage was calculated from 1km buffer.

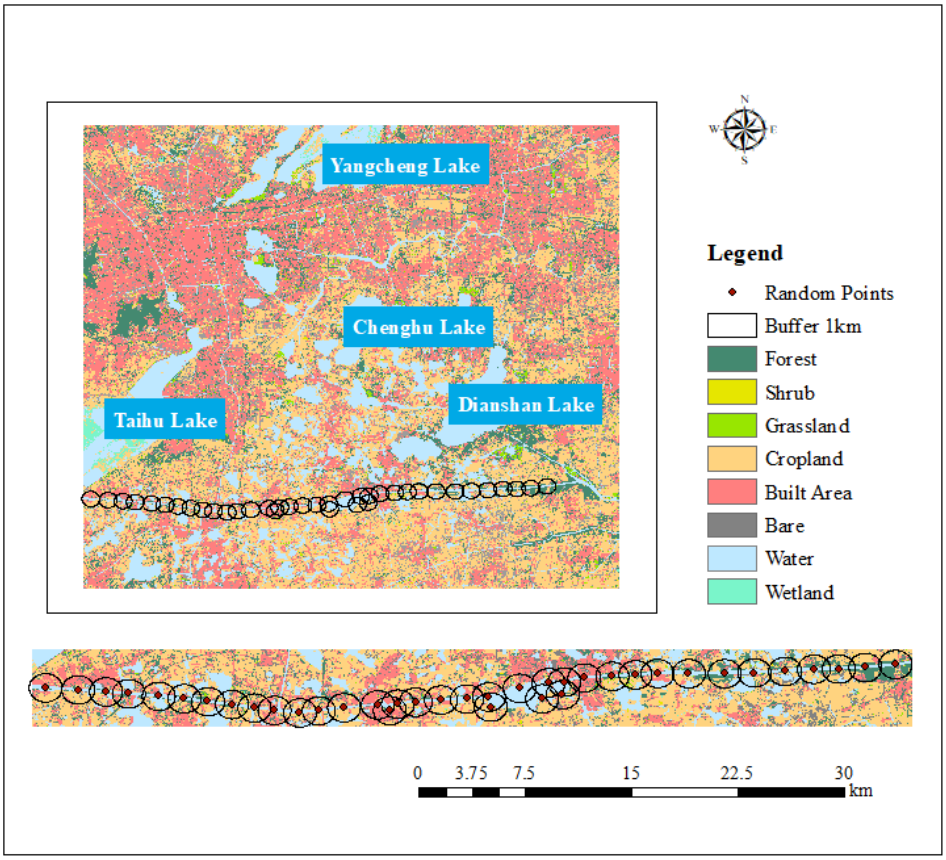

Figure 6 1km buffer zones and land cover types in the Taipu River.

Diagrams derived from redundancy analysis using water quality parameters (red solid lines) and land cover metrics (black solid lines) from 1km buffers were shown in Figure 7. The angles between lines indicate the degree of correlation between individual variables, and the stronger the correlation, the smaller the angle. In addition, the acute angle between the two lines indicates a positive correlation, the obtuse angle indicates a negative correlation. The length of the lines represented the contribution of each land cover index to the water quality variables. Obviously, the narrow angles between TN and cropland indicated that cropland was primarily responsible for the negative effects on TN concentration. In particular, there has been a rise in the usage of herbicides and fertilizers in the last decades. Therefore, rapidly rising amounts of relevant pollutants have entered the river through precipitation and runoff (Xu et al., 2016). The narrow angles between three of the indicators (TP, NH_3-N, and NO_3-N) and built area indicated that built area was primarily responsible for the negative effects on TP, NH_3-N, and NO_3-N. Pollution from built area is a result of urban functions. Built-up areas are extremely likely to have a negative impact on the river's water quality due to the discharge of residential and industrial sewage (Wilson & Weng, 2010). The large angle between the four water quality parameters and forest indicated that forest was primarily responsible for the beneficial effects on all the water quality parameters. Due to plant roots' capacity to absorb nitrogen, phosphorus, and organic matter, as well as soil microbes' ability to decompose organic matter, the forest has a good purifying effect on water quality than built area and cropland .

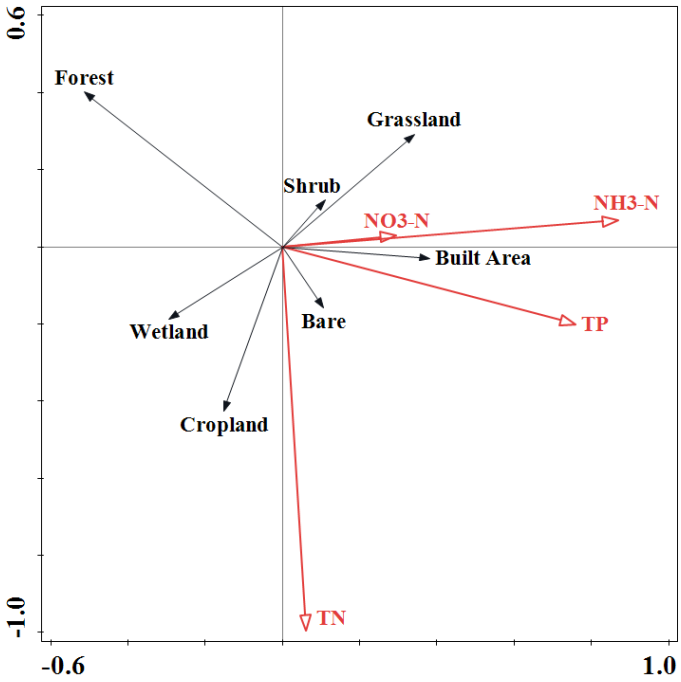

Figure 7 Redundancy analysis diagram in 1km buffer zones and proportion of land use/cover types in the Taipu River. (For interpretation of the references to colour in this figure legend, the reader is referred to the Web version of this article.)

B. Sensitive Bands of Non-optical Parameters between OHS and Sentinel-2

In recent years, hyperspectral technology has become increasingly mature, and it offers new options for water environmental monitoring. In hyperspectral remote sensing, spectral signatures are usually high dimensional, which supports the identification of elements or the measurement of concentrations (Krutz et al., 2019). Therefore, hyperspectral remote sensing technology is more suitable for complex inland bodies of water with non-optical characteristics. The OHS hyperspectral dataset which consists of 2.5nm spectral intervals, represents the target with continuous spectrum throughout the visible and NIR regions. It is more helpful for extracting the subtle spectral differences between water quality parameters (Zhang et al., 2021). In this study, Sentinel-2 and OHS were direct compared to provide more evidence on the potential of the hyperspectral data to retrieve water quality. By comparing the results in Table 3 and Table 4, it was found that the hyperspectral dataset generated higher accuracy models than the multispectral dataset in all cases. It is also shown that the feature bands of water quality retrieval were all comprise by ratio bands, which can reduce the impact of environmental factors to increase the accuracy of the analysis. The combination of green-NIR ratio and Red edge-NIR ratio were most sensitive to TN. The combination of NIR(940nm)-NIR(820nm) ratio and NIR(806nm)-NIR(926nm) ratio were most sensitive to TP. The combination of Red edge-NIR ratio and Red edge-Red ratio were most sensitive to NH_3-N. The combination of Red(596nm)-Red(665nm) ratio and R Blue-Red ratio were most sensitive to NO_3-N. It is also mentioned that the combination of Red edge-Blue ratio and SWIR1-Blue ratio derived from Sentinel-2 image also showed promising results of NO_3-N estimation. That means the SWIR

spectral region (OHS is not available) is critical for detecting NO_3-N concentration.

C. Limitations of the Models

The empirical method uses statistical regression models to link remotely sensed data (single bands or band ratios) to in-situ water quality parameters. It is widely used in remote sensing studies for inland water quality inversion, because it is simple and can be refined by selecting more sensitive spectral bands to improve water quality retrieval accuracy(Li et al., 2017). The results of empirical model indicated that TN、TP、NH_3-N and NO_3-N are highly correlated with OHS spectral data with R^2 ranging from 0.76 to 0.79. The Artificial Intelligence (AI) mode (AIM) concentrates on learning-from-data algorithms and, as a result, generates highly representative features to make linear and non-linear predictions for new unseen data. AIM can also outperform traditional empirical models, which rely heavily on band selection and band combinations. Many researchers have used the AIM mode in water quality retrieval, such as neural networks (NN), support vector machines (SVM), and deep learning (DL), and achieved relatively satisfying results (Chebud et al., 2012; Leong et al., 2019; Pyo et al., 2019). Although the AIM has demonstrated some apparent improvements in assessing water quality, there is an overfitting problem when the sample is not adequate. The AIM cannot be employed in this study since the number of sampling points is limited. The comparison between the empirical model and the AIM is put forward for future research studies.

VI. CONCLUSION

Hyperspectral remote sensing, especially Zhuhai-1 satellite, is an emerging area for monitoring non-optically active water quality parameters, which requires a significant amount of investigation and development in terms of both methods and applications. In this study, we examined four empirical models (linear, logarithmic, exponential and polynomial) for inversion of water quality parameters from the newly available hyperspectral OHS imagery and Sentinel-2 imagery in Taipu River. The evaluation results indicated that OHS performed better than Sentinel-2 for estimating TN, TP, NH_3-N and NO_3-N. This study also demonstrated that the polynomial model based on band ratios performed best for estimating water quality parameters. The band ratios of R(510)/R(820) and R(700)/R(806) performed the best retrieval of TN with R^2 = 0.9678. The band ratios of R(940)/R(820) and R(806)/R(926) performed the best retrieval of TP with R^2 = 0.7924. The band ratios of R(709)/R(806) and R(746)/R(620) performed the best retrieval of NH_3-N with R^2 = 0.7682. The band ratios of R(596)/R(665) and R(466)/R(580) performed the best retrieval of NO_3-N with R^2 = 0.9791. It is worth mentioning that the band ratio of Red Eage3/Blue and SWIR1/Blue of Sentinel-2 also performed well for NO_3-N inversion with R^2 = 0.9513.

The OHS-based empirical models were found acceptable and applicable in estimating water quality parameters of Taipu River. The spatial distribution of TN and NO_3-N shows a general trend of deterioration in the water quality of the Taipu River from upstream to downstream. The TP and NH_3-N concentration is evenly distributed, while all the values of water quality were relatively low across the whole Taipu River. The RDA was applied to analyze the drivers of the spatial distribution of water quality in the Taipu River. The results demonstrated that the proportion of built-up area was significantly positively correlated with TP, NH_3-N and NO_3-N, and cropland was

significantly positively correlated with TN. The proportion of forest was significantly negatively correlated with TN, TP, NH_3-N and NO_3-N. In future studies, the AI models will be investigated to unlock the new opportunities of OHS data in large-scale area water quality inversion.

CRediT authorship contribution statement

Yukun Lin: Conceptualization, Methodology, Software, Writing – original draft, Writing – review & editing, Project administration. Yaojen Tu: Conceptualization, Investigation, Resources, Data Curation, Writing – Review & Editing. Wenpeng Lin: Conceptualization, Writing – review & editing. Weiyue Li: Resources, Writing – Review & Editing. Qianwen Cheng: Software, Writing – review & editing.

Declaration of Competing Interest

The authors declare that they have no known competing financial interests or personal relationships that could have appeared to influence the work reported in this paper.

Acknowledgments

This work was supported by the National Natural Science Foundation of China [grant number 41730642], the Central Guidance on Local Science and Technology Development Fund of Shanghai [grant number YDZX20213100002003] and the Shanghai Natural Science Foundation [grant number 20ZR1441100].

References

Arıman, S. (2021). Determination of inactive water quality variables by MODIS data: A case study in the Kızılırmak Delta-Balik Lake, Turkey. *Estuarine, Coastal and Shelf Science*, *260*, 107505. https://doi.org/https://doi.org/10.1016/j.ecss.2021.107505

Cao, Q., Yu, G., Sun, S., Dou, Y., Li, H., & Qiao, Z. (2022). Monitoring Water Quality of the Haihe River Based on Ground-Based Hyperspectral Remote Sensing. In *Water* (Vol. 14, Issue 1). https://doi.org/10.3390/w14010022

Cao, Y., Ye, Y., Zhao, H., Jiang, Y., Wang, H., Shang, Y., & Wang, J. (2018). Remote sensing of water quality based on HJ-1A HSI imagery with modified discrete binary particle swarm optimization-partial least squares (MDBPSO-PLS) in inland waters: A case in Weishan Lake. *Ecological Informatics*, *44*, 21–32. https://doi.org/https://doi.org/10.1016/j.ecoinf.2018.01.004

Chebud, Y., Naja, G. M., Rivero, R. G., & Melesse, A. M. (2012). Water Quality Monitoring Using Remote Sensing and an Artificial Neural Network. *Water, Air, & Soil Pollution*, *223*(8), 4875–4887. https://doi.org/10.1007/s11270-012-1243-0

Chen, B. T., Mu, X., Chen, P., Wang, B. A., Choi, J., Park, H., Xu, S., Wu, Y. L., & Yang, H. (2021). Machine learning-based inversion of water quality parameters in typical reach of the urban river by UAV multispectral data. *ECOLOGICAL INDICATORS*, *133*. https://doi.org/10.1016/j.ecolind.2021.108434

Chen, X., Wang, Y., Ye, C., Zhou, W., Cai, Z., Yang, H., & Han, X. (2018). Atmospheric Nitrogen Deposition Associated with the Eutrophication of Taihu Lake. *Journal of Chemistry*, *2018*, 4017107. https://doi.org/10.1155/2018/4017107

Donchyts, G., Schellekens, J., Winsemius, H., Eisemann, E., & Van de Giesen, N. (2016). A 30 m Resolution Surface Water Mask Including Estimation of Positional and Thematic Differences Using Landsat 8, SRTM and OpenStreetMap: A Case Study in the Murray-Darling Basin, Australia. In *Remote Sensing* (Vol. 8, Issue 5). https://doi.org/10.3390/rs8050386

Dong, G., Hu, Z., Liu, X., Fu, Y., & Zhang, W. (2020). Spatio-Temporal Variation of Total Nitrogen and Ammonia Nitrogen in the Water Source of the Middle Route of the South-To-North Water Diversion Project. *WATER*, *12*(9). https://doi.org/10.3390/w12092615

Guo, H., Tian, S., Jeanne Huang, J., Zhu, X., Wang, B., & Zhang, Z. (2022). Performance of deep learning in mapping water quality of Lake Simcoe with long-term Landsat archive. *ISPRS Journal of Photogrammetry and Remote Sensing*, *183*, 451–469. https://doi.org/https://doi.org/10.1016/j.isprsjprs.2021.11.023

Guo, H. W., Huang, J. J., Chen, B. W., Guo, X. L., & Singh, V. P. (2021). A machine learning-based strategy for estimating non-optically active water quality parameters using Sentinel-2 imagery. *INTERNATIONAL JOURNAL OF REMOTE SENSING*, *42*(5), 1841–1866. https://doi.org/10.1080/01431161.2020.1846222

Huete, A., Didan, K., Miura, T., Rodriguez, E. P., Gao, X., & Ferreira, L. G. (2002). Overview of the radiometric and biophysical performance of the MODIS vegetation indices. *Remote Sensing of Environment*, *83*(1–2), 195–213.

Irish, R. R., Barker, J. L., Goward, S. N., & Arvidson, T. (2006). Characterization of the Landsat-7 ETM+ automated cloud-cover assessment (ACCA) algorithm. *Photogrammetric Engineering & Remote Sensing*, *72*(10), 1179–1188.

Kallio, K., Kutser, T., Hannonen, T., Koponen, S., Pulliainen, J., Vepsäläinen, J., & Pyhälahti, T. (2001). Retrieval of water quality from airborne imaging spectrometry of various lake types in different seasons. *Science of The Total Environment*, *268*(1), 59–77. https://doi.org/https://doi.org/10.1016/S0048-9697(00)00685-9

Krutz, D., Müller, R., Knodt, U., Günther, B., Walter, I., Sebastian, I., Säuberlich, T., Reulke, R., Carmona, E., Eckardt, A., Venus, H., Fischer, C., Zender, B., Arloth, S., Lieder, M., Neidhardt, M., Grote, U., Schrandt, F., Gelmi, S., & Wojtkowiak, A. (2019). The Instrument Design of the DLR Earth Sensing Imaging Spectrometer (DESIS). In *Sensors* (Vol. 19, Issue 7). https://doi.org/10.3390/s19071622

Leong, W. C., Bahadori, A., Zhang, J., & Ahmad, Z. A. (2019). Prediction of water quality index (WQI) using support vector machine (SVM) and least square-support vector machine (LS-SVM). *International Journal of River Basin Management*, *19*, 149–156.

Li, Y., Zhang, Y., Shi, K., Zhu, G., Zhou, Y., Zhang, Y., & Guo, Y. (2017). Monitoring spatiotemporal variations in nutrients in a large drinking water reservoir and their relationships with hydrological and meteorological conditions based on Landsat 8 imagery. *Science of The Total Environment*, *599–600*, 1705–1717. https://doi.org/https://doi.org/10.1016/j.scitotenv.2017.05.075

Liang, Z., Chen, H., Wu, S., Zhang, X., Yu, Y. H., & Liu, Y. (2018). Exploring Dynamics of the Chlorophyll a-Total Phosphorus Relationship at the Lake-Specific Scale: a Bayesian Hierarchical

Model. *Water, Air, and Soil Pollution*, *229*(1). https://doi.org/10.1007/s11270-017-3678-9

Liu, C., Qian, B. J., Wang, L. Y., & Mao, Q. (2019). Application of GIS and Remote Sensing in Spatial Distribution of Nitrogen and Phosphorus Pollutant in Urban Rivers: A Case Study of Linyi Economic Development Zone, China. *JOURNAL OF COASTAL RESEARCH*, 250–256. https://doi.org/10.2112/SI93-033.1

Liu, J., Zhang, Y., Yuan, D., & Song, X. (2015). Empirical Estimation of Total Nitrogen and Total Phosphorus Concentration of Urban Water Bodies in China Using High Resolution IKONOS Multispectral Imagery. In *Water* (Vol. 7, Issue 11, pp. 6551–6573). https://doi.org/10.3390/w7116551

Lv, J., & Wu, Y. (2021). Nitrogen removal by different riparian vegetation buffer strips with different stand densities and widths. *Water Supply*, *21*(7), 3541–3556. https://doi.org/10.2166/ws.2021.119

Mararakanye, N., Le Roux, J. J., & Franke, A. C. (2022). Long-term water quality assessments under changing land use in a large semi-arid catchment in South Africa. *Science of The Total Environment*, *818*, 151670. https://doi.org/https://doi.org/10.1016/j.scitotenv.2021.151670

Marshak, C., Simard, M., Denbina, M., Nilsson, J., & Van der Stocken, T. (2020). Orinoco: Retrieving a River Delta Network with the Fast Marching Method and Python. In *ISPRS International Journal of Geo-Information* (Vol. 9, Issue 11). https://doi.org/10.3390/ijgi9110658

Pyo, J., Duan, H., Baek, S., Kim, M. S., Jeon, T., Kwon, Y. S., Lee, H., & Cho, K. H. (2019). A convolutional neural network regression for quantifying cyanobacteria using hyperspectral imagery. *Remote Sensing of Environment*, *233*, 111350. https://doi.org/https://doi.org/10.1016/j.rse.2019.111350

Qin, P., Cai, Y., & Wang, X. (2022). Small Waterbody Extraction With Improved U-Net Using Zhuhai-1 Hyperspectral Remote Sensing Images. *IEEE Geoscience and Remote Sensing Letters*, *19*, 1–5.

Qiu, S., Zhu, Z., & He, B. (2019). Fmask 4.0: Improved cloud and cloud shadow detection in Landsats 4-8 and Sentinel-2 imagery. *Remote Sensing of Environment*.

Ross, M. R. V, Topp, S. N., Appling, A. P., Yang, X., Kuhn, C., Butman, D., Simard, M., & Pavelsky, T. M. (2019). AquaSat: A Data Set to Enable Remote Sensing of Water Quality for Inland Waters. *Water Resources Research*, *55*(11), 10012–10025. https://doi.org/https://doi.org/10.1029/2019WR024883

Shi, J., Shen, Q., Yao, Y., Li, J., Chen, F., Wang, R., Xu, W., Gao, Z., Wang, L., & Zhou, Y. (2022). Estimation of Chlorophyll-a Concentrations in Small Water Bodies: Comparison of Fused Gaofen-6 and Sentinel-2 Sensors. *Remote Sensing*, *14*(1). https://doi.org/10.3390/rs14010229

Shi, K., Zhang, Y., Zhu, G., Qin, B., & Pan, D. (2018). Deteriorating water clarity in shallow waters: Evidence from long term MODIS and in-situ observations. *International Journal of Applied Earth Observation and Geoinformation*, *68*, 287–297. https://doi.org/https://doi.org/10.1016/j.jag.2017.12.015

Song, K. S., Li, L., Tedesco, L., Li, S., Shi, K., & Hall, B. (2014). Remote Estimation of Nutrients for a

Drinking Water Source Through Adaptive Modeling. *WATER RESOURCES MANAGEMENT*, *28*(9), 2563–2581. https://doi.org/10.1007/s11269-014-0627-x

Sun, D., Qiu, Z., Li, Y., Shi, K., & Gong, S. (2014). Detection of Total Phosphorus Concentrations of Turbid Inland Waters Using a Remote Sensing Method. *Water, Air, & Soil Pollution*, *225*(5), 1953. https://doi.org/10.1007/s11270-014-1953-6

Sun, X., Zhang, Y., Shi, K., Zhang, Y., Li, N., Wang, W., Huang, X., & Qin, B. (2022). Monitoring water quality using proximal remote sensing technology. *Science of The Total Environment*, *803*, 149805. https://doi.org/https://doi.org/10.1016/j.scitotenv.2021.149805

Toming, K., Kutser, T., Laas, A., Sepp, M., Paavel, B., & Nõges, T. (2016). First Experiences in Mapping Lake Water Quality Parameters with Sentinel-2 MSI Imagery. *Remote Sensing*, *8*(8). https://doi.org/10.3390/rs8080640

Wang, S., Shen, M., Liu, W., Ma, Y., Shi, H., Zhang, J., & Liu, D. (2022). Developing remote sensing methods for monitoring water quality of alpine rivers on the Tibetan Plateau. *GIScience & Remote Sensing*, *59*(1), 1384–1405. https://doi.org/10.1080/15481603.2022.2116078

Wang, X. L., Fu, L., & He, C. S. (2011). Applying support vector regression to water quality modelling by remote sensing data. *INTERNATIONAL JOURNAL OF REMOTE SENSING*, *32*(23), 8615–8627. https://doi.org/10.1080/01431161.2010.543183

Wang, Y., He, B., Duan, W., Li, W., Luo, P., & Razafindrabe, B. H. N. (2016). Source apportionment of annual water pollution loads in river basins by remote-sensed land cover classification. *Water (Switzerland)*, *8*(9), 1–14. https://doi.org/10.3390/w8090361

Wang, Y., Li, F., Mao, L., Chen, M., Tao, H., & Li, J. (2021). Spatial Distribution and Pollution Assessment of Potentially Toxic Elements (PTEs) in Surface Sediments at the Drinking Water Source Channel of Taipu River in China. In *Minerals* (Vol. 11, Issue 11). https://doi.org/10.3390/min11111202

Wang, Z., Wei, L., He, C., & Lu, Q. (2021). Ammonia Nitrogen Monitoring of Urban Rivers with UAV-Borne Hyperspectral Remote Sensing Imagery. *2021 IEEE International Geoscience and Remote Sensing Symposium IGARSS*, 3713–3716. https://doi.org/10.1109/IGARSS47720.2021.9554632

Wilson, C., & Weng, Q. (2010). Assessing Surface Water Quality and Its Relation with Urban Land Cover Changes in the Lake Calumet Area, Greater Chicago. *Environmental Management*, *45*(5), 1096–1111. https://doi.org/10.1007/s00267-010-9482-6

Xu, J., Li, Z., Chi, H., Wang, M., Guan, C., Reiff-Marganiec, S., & Shen, H. (2016). Optimized Composite Service Transactions through Execution Results Prediction. *2016 IEEE International Conference on Web Services (ICWS)*, 690–693. https://doi.org/10.1109/ICWS.2016.107

Yang, H., Kong, J., Hu, H., Du, Y., Gao, M., & Chen, F. (2022). A Review of Remote Sensing for Water Quality Retrieval: Progress and Challenges. In *Remote Sensing* (Vol. 14, Issue 8). https://doi.org/10.3390/rs14081770

Yang, X., Qin, Q., Grussenmeyer, P., & Koehl, M. (2018). Urban surface water body detection with

suppressed built-up noise based on water indices from Sentinel-2 MSI imagery. *Remote Sensing of Environment*, *219*(October), 259–270. https://doi.org/10.1016/j.rse.2018.09.016

Yao, H., Qian, X., Gao, H., Wang, Y., & Xia, B. (2014). Seasonal and Spatial Variations of Heavy Metals in Two Typical Chinese Rivers: Concentrations, Environmental Risks, and Possible Sources. In *International Journal of Environmental Research and Public Health* (Vol. 11, Issue 11, pp. 11860–11878). https://doi.org/10.3390/ijerph111111860

Yao, H., Qian, X., Yin, H., Gao, H., & Wang, Y. (2015). Regional Risk Assessment for Point Source Pollution Based on a Water Quality Model of the Taipu River, China. *RISK ANALYSIS*, *35*(2), 265–277. https://doi.org/10.1111/risa.12259

Zhang, X. W., Zhang, J. C., Chen, W. Y., Liu, W., Zhang, Z. J., Fan, J. W., Xiao, C. J., & Wang, R. (2021). Semi-automated extraction of surface water based on ZhuHai-1 hyperspectral satellite images. *REMOTE SENSING LETTERS*, *12*(8), 750–756. https://doi.org/10.1080/2150704X.2021.1934593

Zhong, Y., Wang, X., Wang, S., & Zhang, L. (2021). Advances in spaceborne hyperspectral remote sensing in China. *Geo-Spatial Information Science*, *24*(1), 95–120. https://doi.org/10.1080/10095020.2020.1860653

Zhu, H. (2018). Distribution and control countermeasures for antimony in water source of Huangpu River upper stream. *Water Purif. Technol*, *37*, 25–32.

Zhu, Z., Wang, S., & Woodcock, C. E. (2015). Improvement and expansion of the Fmask algorithm: cloud, cloud shadow, and snow detection for Landsats 4–7, 8, and Sentinel 2 images. *Remote Sensing of Environment*, *159*, 269–277. https://doi.org/https://doi.org/10.1016/j.rse.2014.12.014